Journal of Power and Energy Engineering, 2025, 13(8), 321-335
https://www.scirp.org/journal/jpee
ISSN Online: 2327-5901
ISSN Print: 2327-588X

Effect of Layer Thickness and Recombination on Charge Transport in 1D Perovskite Solar Cell Models

Rahifa Ranom[1*], Saidatul Nuraisyahtun Sakinah Ahmad Jamal[1], Habibah Ummu[2]

[1]Faculty of Electrical Technology and Engineering, Universiti Teknikal Malaysia Melaka (UTeM), Melaka, Malaysia
[2]Mathematics Department, Brawijaya University, East Java, Indonesia
Email: *rahifa@utem.edu.my

How to cite this paper: Ranom, R., Ahmad Jamal, S.N.S. and Ummu, H. (2025) Effect of Layer Thickness and Recombination on Charge Transport in 1D Perovskite Solar Cell Models. *Journal of Power and Energy Engineering*, **13**, 321-335.
https://doi.org/10.4236/jpee.2025.138018

Received: July 30, 2025
Accepted: August 26, 2025
Published: August 29, 2025

Abstract

Perovskite solar cells (PSCs) have demonstrated remarkable efficiency gains over the past decade. However, their performance remains limited by instability issues arising from environmental factors such as humidity, illumination, and temperature, which affect the charge transport processes within the device. Modelling PSCs is particularly challenging due to the complex and dynamic nature of their physical behaviour, requiring detailed consideration of multiple interdependent parameters. This study focuses on modelling the blend-phase layer of an n-i-p structured perovskite solar cell using a one-dimensional drift-diffusion approach which provides a more physically accurate representation of charge carrier dynamics. The coupled equations are solved numerically using the Method of Lines (MOL) technique, which enables efficient temporal integration of spatially discretized equations. Key parameters such as active layer thickness and the bimolecular recombination coefficient are varied to assess their influence on cell performance. Simulation results indicate that the highest observed efficiency is achieved at a perovskite layer thickness of 500 nm with a recombination coefficient of $b_1 = 1\times10^{-10}\ \mathrm{m}^3\cdot\mathrm{s}^{-1}$.

Keywords

Perovskite Solar Cell, Drift-Diffusion, Thickness, Recombination, Efficiency

1. Introduction

Semiconductors have become essential in photovoltaic (PV) technologies due to their ability to directly convert sunlight into electrical energy. Among various PV technologies, perovskite solar cells (PSCs) have drawn significant attention for

their high power conversion efficiency, low manufacturing cost, and compatibility with low-temperature, solution-based fabrication methods [1] [2]. Unlike conventional silicon-based solar cells, PSCs offer easier processing and the potential for higher efficiencies, with reports of over 25% efficiency in recent years [1] [3]. However, key challenges such as environmental instability, degradation under moisture and heat, and current-voltage hysteresis still hinder large-scale commercialization [4] [5].

The performance and stability of PSCs are strongly influenced by charge transport dynamics within their layered structure, typically consisting of a Hole Transport Layer (HTL), a perovskite absorber, and an Electron Transport Layer (ETL). Charge transport is governed by drift due to internal electric fields and diffusion driven by carrier concentration gradients [6]. Moreover, interfacial effects, including ion migration and charge accumulation, contribute to hysteresis and performance losses [7] [8]. To gain insight into these mechanisms, one-dimensional drift-diffusion models are widely used, incorporating effects such as light-induced carrier generation and potential barriers at interfaces [9]-[11]. This study investigates the steady-state behaviour of a three-layer PSC by numerically solving the coupled drift-diffusion equations, aiming to better understand charge carrier dynamics and their impact on overall device performance.

Modelling solar cell operation involves solving a set of coupled nonlinear partial differential equations that describe key physical mechanisms such as photogeneration, charge carrier transport via drift and diffusion, recombination, and interfacial effects across multiple material layers. These models incorporate numerous parameters; including carrier mobilities, lifetimes, dielectric constants, and built-in potentials which contribute to their mathematical complexity and sensitivity to boundary and initial conditions [12] [13]. Despite this complexity, many existing studies simplify the modelling by assuming steady-state conditions and neglecting temporal effects, thus overlooking critical phenomena such as hysteresis, ion migration, and transient responses under dynamic illumination or biasing conditions [5] [14]. This research was explicitly solving time dependence of the charge transport equations, enabling a more realistic analysis of dynamic processes in perovskite solar cells. Although the results presented are steady state, the time-dependent drift-diffusion equations were solved to capture the cell transient behaviour before the cell reached steady state. This study contributes toward SDG 7: Affordable and Clean Energy by providing insights that support the development of high-efficiency, stable perovskite solar cells through improved numerical modelling and device optimization.

2. Modelling of Perovskite Solar Cell

Modelling the perovskites solar required the understanding of the working principle of the solar cell. The basic mechanisms of the solar cell consist of different types of processes, that are the generation process, transportation process, and collection process. The operation of perovskite solar cell is shown in **Figure 1**.

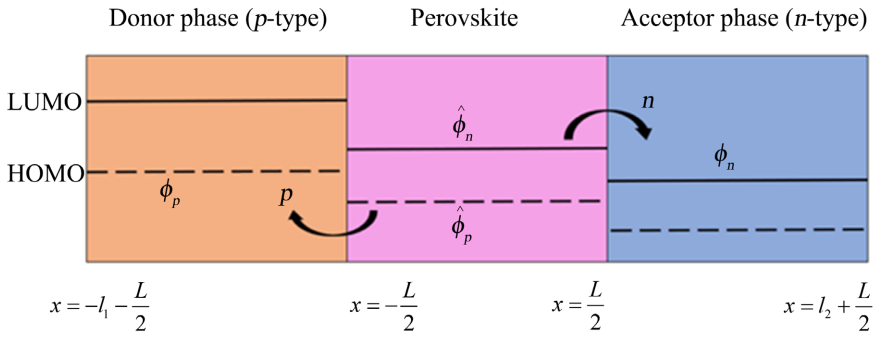

Figure 1. The schematic diagram of the perovskites solar cell. The dashed line represents the highest occupied molecular orbital (HOMO) (solid line) while the least unoccupied molecular orbital (LUMO) (dashed line). The *p*-type donor layer ($-l_1-\frac{L}{2}<x<-\frac{L}{2}$), the perovskite layer ($-\frac{L}{2}<x<\frac{L}{2}$) and the *n*-type acceptor layer ($\frac{L}{2}<x<l_2+\frac{L}{2}$). The *p* denotes as hole and *n* denotes as electron, where x represents thickness and L is diffusion length. HTL is a *p*-type layer made up of spiro-OMETAD consisting of hole charge while the blend phase layer (perovskites) consisted of holes and electron charge, and ETL is a *n*-type layer made up of titanium oxide (TiO_2) which is filled by electrons charge.

Figure 1 shows the mechanism of a perovskite solar cell. In the perovskite solar cell, the structure of the perovskite layer acts as a blend phase layer ($-\frac{L}{2}<x<\frac{L}{2}$) is sandwiched between the *p*-type donor layer ($-l_1-\frac{L}{2}<x<-\frac{L}{2}$), and the *n*-type acceptor layer ($\frac{L}{2}<x<l_2+\frac{L}{2}$). The sunlight is absorbed in the perovskite layer that has a highly ordered crystalline structure comprised of distinct conduction band edges, $\hat{\phi}_n$, and valence band edges, $\hat{\phi}_p$ that are divided by a band gap. Furthermore, the organics materials of the donor phase (*p*-type) and acceptor phase (*n*-type) have no distinct band structure and are amorphous. LUMO portrays the conduction band, and the energy of the acceptor is denoted as ϕ_n while HOMO portrays the valence band, and the energy of the donor is denoted as ϕ_p. The electrons are excited into the LUMO, leaving a hole in the HUMO, resulting in the conduction process due to the excited electrons and hole movement between the HUMO and LUMO respectively on the adjacent molecules. This process is commonly known as hopping between shallows and traps for highly localized energy wells.

The Drift-Diffusion Equations in Perovskite Layer and the Boundary Conditions

The conservation of electrons and hole densities in perovskite layer ($-\frac{L}{2}<x<\frac{L}{2}$) are defined as:

$$\frac{\partial p}{\partial t}+\frac{\partial}{\partial x}\left(-D_p\left(\frac{\partial p}{\partial x}-\frac{pq}{kT}\frac{\partial \phi}{\partial x}\right)\right)=b\left(np-N_i^2\right), \tag{1}$$

$$\frac{\partial n}{\partial t}-\frac{\partial}{\partial x}\left(D_n\left(\frac{\partial n}{\partial x}-\frac{nq}{kT}\frac{\partial \phi}{\partial x}\right)\right)=b\left(np-N_i^2\right), \tag{2}$$

where p represents holes, n is electrons, k is the Boltzmann's constant, q is the elementary charge, whereas T displays the temperature. The temperature is set to be constant at 300 K. The electrons and holes in the absorber layer go through the process of generation and recombination that complies with the concept of conservation of energy in terms of continuity equations. Equation (1) indicates the charge density of holes while Equation (2) is the charge density of electrons. The right-hand side of the Equations (1) and (2) denote the recombination in perovskites which is assumed as bimolecular recombination due to the well-defined crystalline structure of perovskites. A uniform generation rate was assumed and incorporated into the continuity equations to reflect evenly distributed photon absorption across the active layer. The notation of N_i indicates the intrinsic carrier density, while b is the recombination coefficient of the perovskites solar cell. The conservation equations are coupled with Poisson's Equation (3);

$$\frac{\partial^2 \phi}{\partial x^2}=\frac{q\left(n-p\right)}{\epsilon}, \tag{3}$$

where ϵ is the permittivity at the perovskite. The boundary conditions at the interface of perovskite and HTL are written as in Equation (4):

$$p=\alpha_p \pi_0,\ \phi=V_0,\ n_x=-\pi_0 \ \text{ at } x=-\frac{L}{2}, \tag{4}$$

The n_x, is the rate of change of electrons in thickness. At the interface of perovskite and ETL, the boundary conditions for the single-layer model is written as (5):

$$n=\alpha_n \pi_0,\ \phi=-V_0,\ p_x=\pi_0 \ \text{ at } x=\frac{L}{2}. \tag{5}$$

The p_x, is the rate of change of the holes against thickness. The notation of π_0 is the typical charge density required to carry the current of magnitude the typical photo-generated current density. The values of π_0 and V_0 are 7.9×10^{23} m^{-3} and 0.00258 V, respectively [10].

3. Numerical Procedure

This study employs numerical techniques to solve the drift-diffusion equations governing charge transport in perovskite solar cells, with a focus on the Method of Lines (MOL). These equations, which include both partial and ordinary differential equations (PDEs and ODEs), need to be solved over time to demonstrate how the system changes [10] [15]. While commercial solvers such as SCAPS-1D, COMSOL, and Ion Monger are commonly used, they are limited by assumptions and predefined settings [16] [17]. This study focuses specifically on modeling charge transport within the perovskite absorber layer. However, the numerical framework developed here is general and can be extended to include adjacent lay-

ers such as the electron transport layer (ETL) and hole transport layer (HTL), allowing for full device simulations in future work.

Method of Lines (MOL) is a semi-discretization method in which spatial derivatives in Equations (1) - (3) are discretized (assume that the diffusion coefficients of the holes and electrons are constants) to convert the governing PDEs into a system of ordinary differential equations (ODEs) that can be solved using established time integration methods [18]. Discretize Equations (1) - (3) to obtain

$$\frac{\partial p_i}{\partial t} = \frac{D_p}{h^2}\left[p_{i+1} - 2p_i + p_{i-1} + \frac{q}{kT}\frac{\left(p_i + p_{i+1}\right)\left(\varphi_{i+1} - \varphi_i\right) - \left(p_i + p_{i-1}\right)\left(\varphi_i - \varphi_{i-1}\right)}{2}\right] + b\left(n_i p_i - N_i^2\right) \tag{6}$$

$$\frac{\partial n_i}{\partial t} = \frac{D_n}{h^2}\left[n_{i+1} - 2n_i + n_{i-1} - \frac{q}{kT}\frac{\left(n_i + n_{i+1}\right)\left(\varphi_{i+1} - \varphi_i\right) - \left(n_i + n_{i-1}\right)\left(\varphi_i - \varphi_{i-1}\right)}{2}\right] + b\left(n_i p_i - N_i^2\right) \tag{7}$$

$$0 = \frac{1}{h^2}\left[\varphi_{i+1} - 2\varphi_i + \varphi_{i-1}\right] - \frac{q}{\epsilon}\left(n_i - p_i\right) \tag{8}$$

This results in a system of coupled ODEs, where each equation (Equations (6) - (8)) corresponds to a discretized spatial point. These equations describe the time evolution of variables such as electron and hole densities and the electrostatic potential across the device layers;

$$\boldsymbol{M}\frac{\partial \boldsymbol{u}_i}{\partial t} = \boldsymbol{A}\boldsymbol{u} + f\left(x,t\right) \tag{9}$$

The $\boldsymbol{u}_{N\times 1}$ is the solution vector, $\boldsymbol{M}_{N\times N}$ represents the time-dependent mass matrix, $\boldsymbol{A}_{N\times N}$ denotes the differentiation matrix, and the $f\left(x,t\right)$ is the generation and recombination of charge density of holes and electrons, while for the Poisson equation, it is the difference between electrons and holes.

$$\boldsymbol{M} = \begin{bmatrix} M_p & 0 & 0 \\ 0 & M_n & 0 \\ 0 & 0 & 0 \end{bmatrix}_{3N\times 3N}, \boldsymbol{A} = \begin{bmatrix} A_p & 0 & 0 \\ 0 & A_n & 0 \\ 0 & 0 & A_\phi \end{bmatrix}_{3N\times 3N}, f\left(x,t\right) = \begin{bmatrix} f_p \\ f_n \\ f_\phi \end{bmatrix}_{3N\times 1} \tag{10}$$

where p is the system for holes, n is the system for electrons, and ϕ is the system for potential difference.

One major advantage of the MOL is its flexibility and compatibility with various stiff and non-stiff ODE solvers. In this study, the resulting ODE system (Equations (9) - (10)) is solved using MATLAB's ODE15s solver, which is well-suited for stiff systems and those involving singular mass matrices. The MOL method also allows for straightforward incorporation of boundary and initial conditions, and it scales efficiently with increasing spatial resolution, making it an ideal choice for simulating the dynamic behavior of complex, multilayer solar cell structures. The set of parameters for the perovskite solar cell used in this model is tabulated in **Table 1**.

Table 1. Parameter values of the cell.

Symbol	Description	Value
$\check{D}_p$	Diffusion coefficient of holes at perovskite	2.5×10^{-5} m^2·s^{-1}
D_p	Diffusion coefficient of holes at HTL	10×10^{-10} m^2·s^{-1}
D_n	Diffusion coefficient of holes at ETL	2.5×10^{-9} m^2·s^{-1}
q	Elementary charge	1.602×10^{-19} C
b	Recombination rate coefficient	1.1×10^{-16} m^{-3}·s^{-1}
ϵ_p	Permittivity of perovskite	5.7552×10^{-11} F·m^{-1}
ϵ_d	Permittivity of HTL	2.6563×10^{-11} F·m^{-1}
ϵ_a	Permittivity of ETL	7.0834×10^{-10} F·m^{-1}
T	Temperature	300 K
L	Thickness of perovskites	500×10^{-9} m
l_1	Thickness of HTL	500×10^{-9} to 700×10^{-9} m
l_2	Thickness of ETL	50×10^{-9} to 100×10^{-9} m
k	Boltzmann constant	1.38×10^{-23} J·K^{-1}

4. Results and Discussion

The simulation result for the unsteady state condition at the blend phase layer (perovskite layer) is shown in dimensional form. The comparison of the simulation result obtained and the experimental simulation result from Foster *et al.* [19] is shown in Figure 2.

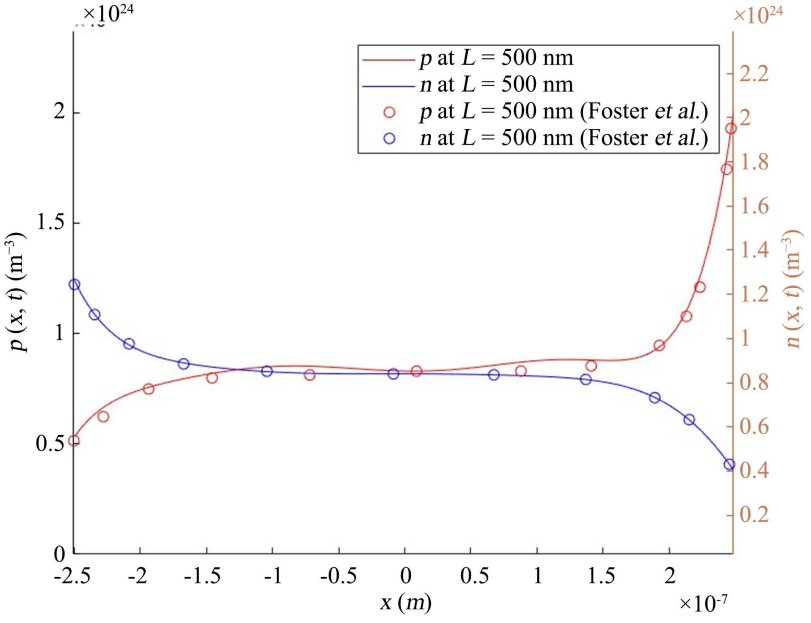

Figure 2. The comparison of the simulation result of charge densities against thickness with the experimental simulation result [19].

Based on the result, the holes and electrons' densities position are almost similar to the reference as the condition referred to by Foster *et al.* [19] is in a steady state condition. The behaviour of the charge densities in **Figure 2** is related to the dynamic mechanism of the perovskite solar cell. At the blend phase layer (perovskite), the absorption of light occurs and excites the electron-hole pair, resulting in the movement of holes and electrons [20] [21]. The electric field produced between HTL and ETL causes the electrons and holes to drift toward the selective layers.

At $x = 250\ \text{nm}$, the value of electron density $(250\ \text{nm}, t)$, becomes 3.9281 × 10^{23} m^{-3} representing the behaviour of photo-generated electrons diffused from the blend phase layer into the ETL. The hole density at $x = 250\ \text{nm}$ has a value of 2.055 × 10^{24} m^{-3}, showing that the accumulation occurs due to the selective charge properties at the interface of the blend phase (perovskite) layer to the ETL [2]. The holes accumulated are then blocked from entering ETL.

At $x = -250\ \text{nm}$, the value of hole density, $p(-250\ \text{nm}, t) = 5.3133 \times 10^{23}\ \text{m}^{-3}$, which is lower compared to the density of electrons. This situation represents a movement of the photo-generated holes from the blend phase (perovskite) layer into HTL. Meanwhile, the value of electron density, $n(-250\ \text{nm}, t)$ piled up to 1.264 × 10^{24} m^{-3} due to the selective layer properties at the interface of the HTL, thus blocking electrons from entering HTL [15]. The result shows that the concentration of charge density is important and can affect the performance of the solar cell. The effect of the parameter variation, such as thickness and the recombination coefficient, is discussed in the next section.

4.1. The Impact of Varying Thickness in the Perovskite Layer

Figure 3 illustrates the spatial distribution of charge carrier densities of electrons $n(x,t)$ and holes $p(x,t)$ within the perovskite layer for five different thicknesses: L = 100 nm, 200 nm, 300 nm, 400 nm, 500 nm. The profiles show that both carrier types exhibit a symmetric distribution across the device, with electron density increasing toward the right interface and hole density increasing toward the left, which is consistent with their respective directions of drift under the internal electric field.

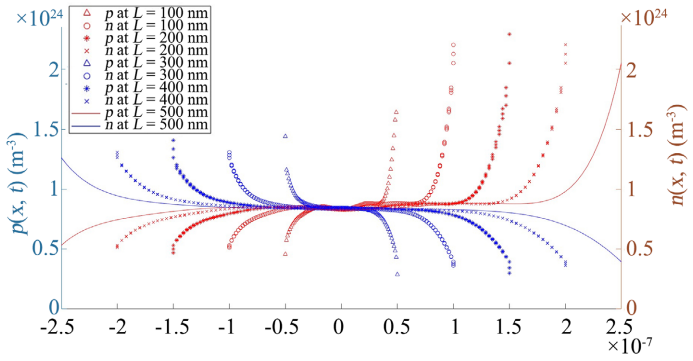

Figure 3. The charge density against thickness at L = 100 nm, 200 nm, 300 nm, 400 nm, 500 nm.

At the center of the device, $x = 0$; $p(x,t)$ reach minimum values, indicating a quasi-neutral region or dominant recombination zone. As the perovskite thickness increases, the gradients of both carrier densities become steeper, and the accumulation near the contacts becomes more pronounced. This behavior suggests that thicker layers enhance field-driven transport but may also lead to increased carrier separation and interface effects. These results highlight the critical role of layer thickness in influencing charge distribution, transport behavior, and, ultimately, the performance of perovskite solar cells. The trends observed are consistent with theoretical expectations from the drift-diffusion model and provide insights for optimizing active layer thickness in device design.

The charge densities of holes and electrons are affected by the thickness and the recombination rate of the perovskite layer as the time, t increases. At the interface of HTL and perovskite layer, $x = -250$ nm for the thickness of 100 nm to 500 nm, the density of holes becomes steeper, showing that there is a movement of holes from the perovskite layer into the HTL. A Debye layer (selective layer) is formed between HTL and perovskite, blocking the electron's movement from entering the HTL.

At the interface of the ETL and the perovskite, $x = 250$ nm, for the thickness of 100 nm to 500 nm, the density of electrons becomes steeper, showing that the movement of electrons from perovskite into the ETL is active. The Debye layer is formed at the interface of ETL and perovskite, allowing only electrons and blocking the hole from passing into ETL.

The concentration of charge density of holes and electrons at thicknesses of 100 nm to 300 nm increased and is reduced starting at 400 nm to 500 nm. The phenomenon is a result of the recombination that happens in the perovskite layer, which is related to the time taken for the charge separation to occur at the interface of the blend phase (perovskite) with ETL and HTL. In other words, the charge density is influenced by the changes in the thickness of the blend phase (perovskite) layer due to the recombination mechanism. At the thickness of 300 nm to 500 nm, the time taken for photo-generated holes and electrons to be diffused toward the selective layer becomes slower compared to a thickness from 100 nm to 300 nm, resulting in the recombination of holes and electrons before reaching the selective contacts.

The relation of the charge density behaviour with different thicknesses of the blend phase layer is studied in terms of efficiency and is simulated via the J-V curve in **Figure 4**.

The charge densities of holes and electrons are affected by the thickness and the recombination rate of the perovskite layer as the time, t increases. At the interface of HTL and perovskite layer, $x = -250$ nm for the thickness of 100 nm to 500 nm, the density of holes becomes steeper, showing that there is a movement of holes from the perovskite layer into the HTL. A Debye layer (selective layer) is formed between HTL and perovskite, blocking the electron's movement from entering the HTL.

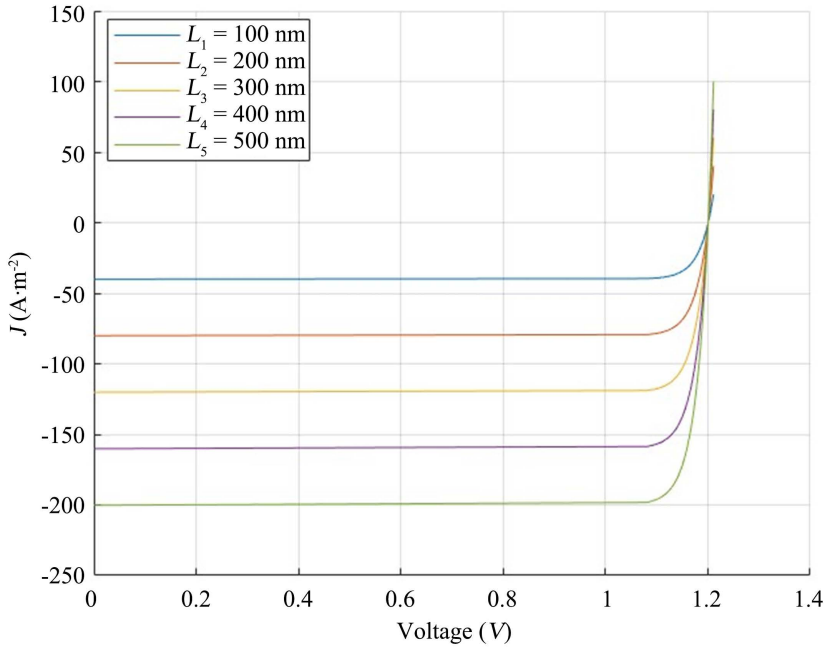

Figure 4. The result of the varied thickness on the J-V curve for the blend phase layer.

At the interface of the ETL and the perovskite, $x = 250$ nm, for the thickness of 100 nm to 500 nm, the density of electrons becomes steeper, showing that the movement of electrons from perovskite into the ETL is active. The Debye layer is formed at the interface of ETL and perovskite, allowing only electrons and blocking the hole from passing into ETL.

The concentration of charge density of holes and electrons at thicknesses of 100 nm to 300 nm increased and is reduced starting at 400 nm to 500 nm. The phenomenon is a result of the recombination that happens in the perovskite layer, which is related to the time taken for the charge separation to occur at the interface of the blend phase (perovskite) with ETL and HTL. In other words, the charge density is influenced by the changes in the thickness of the blend phase (perovskite) layer due to the recombination mechanism. At the thickness of 300 nm to 500 nm, the time taken for photo-generated holes and electrons to be diffused toward the selective layer becomes slower compared to a thickness from 100 nm to 300 nm, resulting in the recombination of holes and electrons before reaching the selective contacts. The relation of the charge density behavior with different thicknesses of the blend phase layer is studied in terms of efficiency and is simulated via the J-V curve in **Figure 4**.

As the thickness increases from 100 nm to 500 nm, the value of the maximum voltage, V_m is reduced from 1.110 V to 1.103 V while the open circuit voltage, V_{oc} remains constant. The efficiency of the perovskite solar cell increases as the thickness of the blend phase increases from 100 nm with an efficiency of 4.31% to 500 nm with an efficiency of 21.59% (as shown in **Table 2**). The phenomenon can be related to the generation and recombination mechanism. In contrast with the charge separation phenomenon, even though the concentration of charge densi-

ties at $L = 100$ nm is high with slow recombination, the area for the light absorption is small compared to $L = 500$ nm . When the thickness becomes higher, the absorption of light area becomes wider, while the excitation of the holes-electrons paired becomes rapid. As a result, the short circuit current density, J_{sc} soared from -40.05 A·m^{-2} to -200.27 A·m^{-2} and the value of the maximum current density, J_m also increased from -38.85 A·m^{-2} to -195.67 A·m^{-2}. The thickness of the perovskite layer affects the time taken for the movement of the charge separation and the efficiency of the perovskite solar cell. This work suggested the thickness of the perovskite solar cell of 500 nm is proven efficient for the optimum charge generation and separation in the perovskite solar cell [7]. While 500 nm yielded the highest efficiency within the simulated range, the increasing trend suggests that the optimum thickness may lie beyond this value. However, other types of recombination should be considered and further research is required for this case.

Table 2. The efficiency of the perovskite solar cell with the varied thickness for the blend phase (perovskite) layer.

The thickness of the blend phase layer, L (nm)	$J_{sc}\left(\mathrm{A\cdot m^{-2}}\right)$	$V_{oc}\left(\mathrm{V}\right)$	$V_{oc}\left(\mathrm{V}\right)$	FF	Efficiency (%)
100	−40.05	1.201	−38.85	0.8968	4.31
200	−80.11	1.201	−78.51	0.8975	8.63
300	−10.16	1.201	−117.76	0.8975	12.95
400	−160.22	1.201	−157.01	0.8975	17.26
500	−200.27	1.201	−195.67	0.8977	21.59

4.2. The Impact of Different Recombination Coefficients in the Perovskite Layer

The simulation result of the impact of different recombination coefficients, b for $b_1 = 1.1\times10^{-10}\ \mathrm{m^3\cdot s^{-1}}$, $b_2 = 2.2\times10^{-14}\ \mathrm{m^3\cdot s^{-1}}$, $b_3 = 1\times10^{-15}\ \mathrm{m^3\cdot s^{-1}}$, and $b_4 = 1.1\times10^{-16}\ \mathrm{m^3\cdot s^{-1}}$ on the charge densities are shown in **Figure 5**.

The results show that at the highest recombination rate ($b_1 = 1\times10^{-10}\ \mathrm{m^3\cdot s^{-1}}$), both carrier concentrations exhibit sharp gradients near the contact interface, indicating strong carrier separation driven by a built-in electric field and effective drift-diffusion transport. This results in a higher open-circuit voltage and device efficiency, as efficient charge extraction outweighs recombination losses. As the recombination coefficient decreases (b_2 to b_4), the charge density profiles become increasingly uniform, reflecting weaker internal electric fields and reduced carrier separation efficiency. Although lower recombination theoretically minimizes losses, the charge density profiles suggest weakened carrier drift and potential accumulation, which contribute to lower photovoltage and fill factor. These results affirm that an optimal recombination coefficient is critical to balance charge separation and transport. The relation of the bimolecular recombination coefficient effect on the performance of the perovskite solar cell in terms of the J-V curve is shown in **Figure 6**.

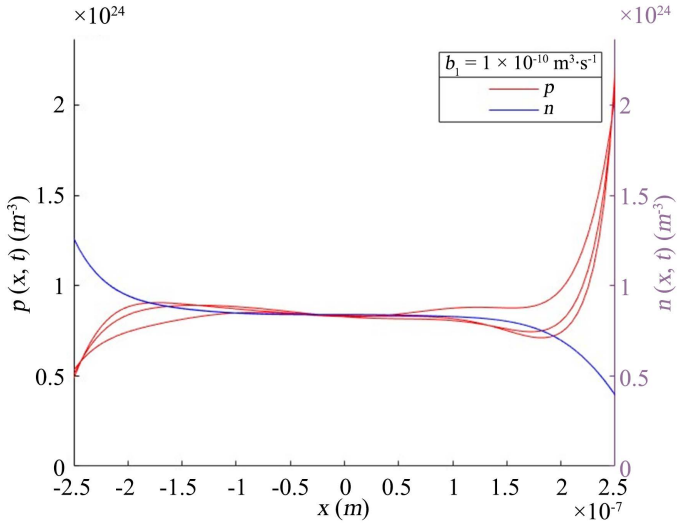
×10^24
×10^24
b1 = 1 × 10^-10 m^3·s^-1
p
n
p (x, t) (m^-3)
n (x, t) (m^-3)
x (m)
×10^-7

(a)

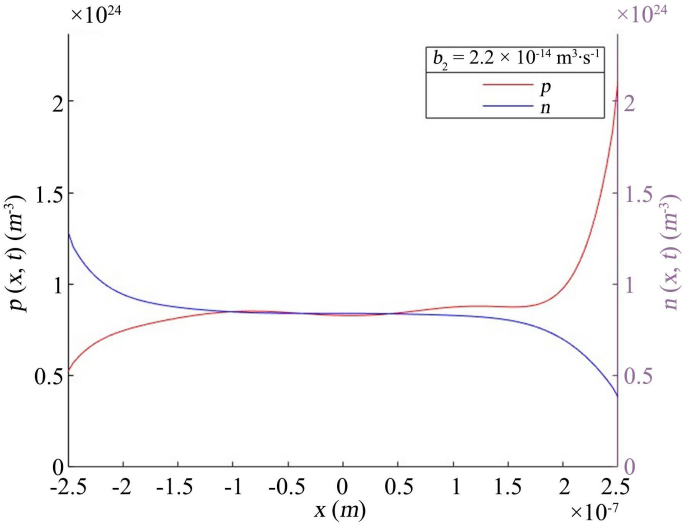
×10^24
×10^24
b2 = 2.2 × 10^-14 m^3·s^-1
p
n
p (x, t) (m^-3)
n (x, t) (m^-3)
x (m)
×10^-7

(b)

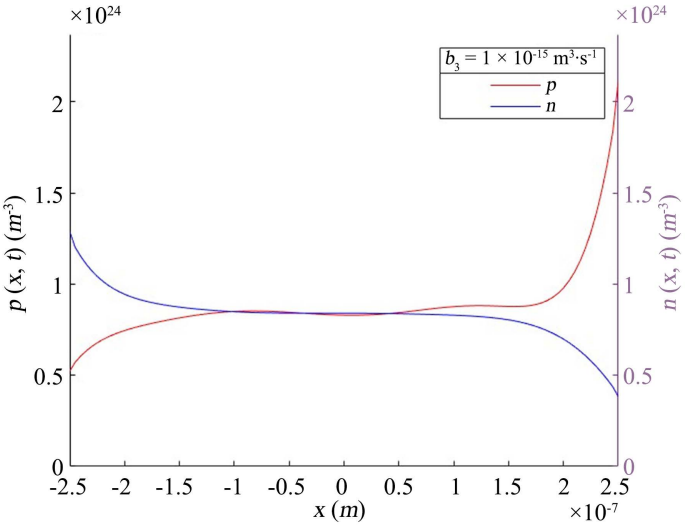
×10^24
×10^24
b3 = 1 × 10^-15 m^3·s^-1
p
n
p (x, t) (m^-3)
n (x, t) (m^-3)
x (m)
×10^-7

(c)

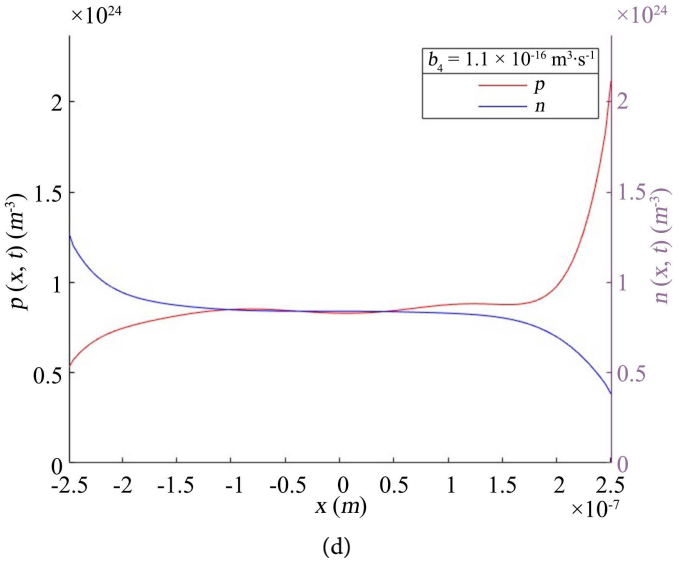

Figure 5. The electron and hole densities against thickness for (a) $b_1 = 1.1\times10^{-10}\ \mathrm{m^3\cdot s^{-1}}$, (b) $b_2 = 2.2\times10^{-14}\ \mathrm{m^3\cdot s^{-1}}$, (c) $b_3 = 1\times10^{-15}\ \mathrm{m^3\cdot s^{-1}}$ and (d) $b_4 = 1.1\times10^{-16}\ \mathrm{m^3\cdot s^{-1}}$.

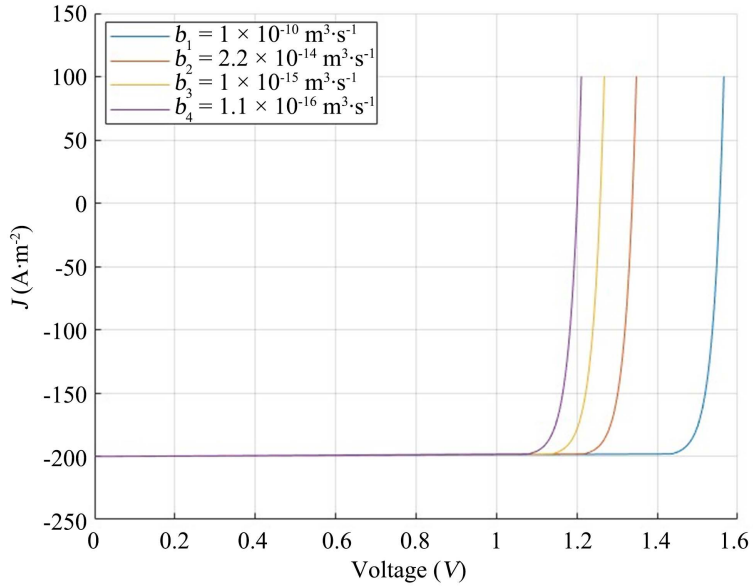

Figure 6. The impact of different recombination coefficients on the performance of the perovskite solar cell.

The efficiency calculation process obtained from the simulation of the J-V curve, as shown in **Figure 6** and tabulated in **Table 3**, reveals the impact of varying recombination coefficients b on the performance of perovskite solar cells. Although the short-circuit current density J_{sc} remains constant at $-200.27\ \mathrm{A\cdot m^{-2}}$, changes in the recombination coefficient significantly affect the open-circuit voltage V_{oc}, fill factor (FF), and the cell efficiency. The efficiency is the highest (28.54%) at $b_1 = 1\times10^{-10}\ \mathrm{m^3\cdot s^{-1}}$, and gradually decreases to 21.59% at $b_4 = 1.1\times10^{-16}\ \mathrm{m^3\cdot s^{-1}}$. It indicates that a moderate level of recombination can bal-

ance carrier density and enhance voltage under certain conditions. In contrast, too low recombination, while reducing carrier losses, may impair electric field distribution and charge separation efficiency, leading to performance degradation as shown in Figure 5. The degradation may occur because suppressing bulk recombination without addressing interface quality or contact selectivity can lead to carrier accumulation and reduced extraction efficiency, hence lowering solar cell performance [22]. It is important to note that these results are obtained by considering the perovskite layer in isolation; without electron transport layer (ETL) and hole transport layer (HTL) which may further influence the cell's recombination dynamics. Regardless of the recombination value, the efficiency reduction reflects the intrinsic limitations of a doped perovskite layer operating without transport layers. The findings also confirm that recombination dynamics directly influence the distribution and density of charge carriers (electrons and holes) in the device, emphasizing the importance of optimizing recombination parameters to achieve higher solar cell performance.

Table 3. The efficiency of the perovskite solar cell with the effect of different recombination coefficients.

Recombination coefficient, $b\left(\mathrm{m}^3\cdot\mathrm{s}^{-1}\right)$	$J_{sc}\left(\mathrm{A}\cdot\mathrm{m}^{-2}\right)$	V_{oc}	FF	Efficiency (%)
1×10^{-10}	−200.27	1.5552	0.9164	28.54
2.2×10^{-14}	−200.27	1.3375	0.9056	24.26
1×10^{-15}	−200.27	1.2577	0.9013	22.70
1.1×10^{-16}	−200.27	1.2006	0.8977	21.59

Acknowledgements

We would like to express our sincere appreciation toward Universiti Teknikal Malaysia Melaka (UTeM) and Center for Robotics and Industrial Automation (CeRIA) for the research support.

Conflicts of Interest

The authors declare no conflicts of interest regarding the publication of this paper.

References

[1] NREL. Best Research-Cell Efficiency Chart. National Renewable Energy Laboratory. https://www.nrel.gov/pv/cell-efficiency.html

[2] Kojima, A., Teshima, K., Shirai, Y. and Miyasaka, T. (2009) Organometal Halide Perovskites as Visible-Light Sensitizers for Photovoltaic Cells. *Journal of the American Chemical Society*, **131**, 6050-6051. https://doi.org/10.1021/ja809598r

[3] Jeong, M., Choi, I.W., Go, E.M., *et al.* (2020) Stable Perovskite Solar Cells with Efficiency Exceeding 24.8% and 0.3-V Voltage Loss. *Science*, **369**, 1615-1620.

[4] Niu, G., Guo, X. and Wang, L. (2015) Review of Recent Progress in Chemical Stability of Perovskite Solar Cells. *Journal of Materials Chemistry A*, **3**, 8970-8980.

https://doi.org/10.1039/c4ta04994b

[5] Tress, W. (2017) Metal Halide Perovskites as Mixed Electronic-Ionic Conductors: Challenges and Opportunities—From Hysteresis to Memristivity. *Journal of Physics: Energy*, **1**, Article ID: 022001. https://doi.org/10.1088/2515-7655/ab1abf

[6] Ravishankar, S., Boobna, P. and Tress, W. (2021) Modeling Charge Transport in Perovskite Solar Cells: A Review. *Advanced Energy Materials*, **11**, Article ID: 2002649.

[7] Yuan, Y. and Huang, J. (2016) Ion Migration in Organometal Trihalide Perovskite and Its Impact on Photovoltaic Efficiency and Stability. *Accounts of Chemical Research*, **49**, 286-293. https://doi.org/10.1021/acs.accounts.5b00420

[8] Kim, H. and Park, N. (2014) Parameters Affecting I-V Hysteresis of $CH_3NH_3PbI_3$ Perovskite Solar Cells: Effects of Perovskite Crystal Size and Mesoporous TiO_2 Layer. *The Journal of Physical Chemistry Letters*, **5**, 2927-2934. https://doi.org/10.1021/jz501392m

[9] Snaith, H.J. (2013) Perovskites: The Emergence of a New Era for Low-Cost, High-Efficiency Solar Cells. *The Journal of Physical Chemistry Letters*, **4**, 3623-3630. https://doi.org/10.1021/jz4020162

[10] Courtier, N.E., Cave, J.M., Foster, J.M., Walker, A.B. and Richardson, G. (2019) How Transport Layer Properties Affect Perovskite Solar Cell Performance: Insights from a Coupled Charge Transport/Ion Migration Model. *Energy & Environmental Science*, **12**, 396-409. https://doi.org/10.1039/c8ee01576g

[11] Guerrero, A., You, J., Aranda, C., Kang, Y.S., Garcia-Belmonte, G., Zhou, H., *et al.* (2015) Interfacial Degradation of Planar Lead Halide Perovskite Solar Cells. *ACS Nano*, **10**, 218-224. https://doi.org/10.1021/acsnano.5b03687

[12] Nelson, J. (2003) The Physics of Solar Cells. Imperial College Press.

[13] Würfel, P. and Würfel, U. (2016) Physics of Solar Cells: From Basic Principles to Advanced Concepts. Wiley-VCH.

[14] Richardson, G., Courtier, N.E., Foster, J.M. and Walker, A.B. (2016) Ion Migration and the Role of Hysteresis in Perovskite Solar Cells: A Coupled Device Model. *Energy & Environmental Science*, **9**, 1476-1486. https://doi.org/10.1039/C5EE03676H

[15] Courtier, N.E. (2020) Interpreting Ideality Factors for Planar Perovskite Solar Cells: Ectypal Diode Theory for Steady-State Operation. *Physical Review Applied*, **14**, Article ID: 024031. https://doi.org/10.1103/physrevapplied.14.024031

[16] Clarke, W., Bennett, L.J., Grudeva, Y., Foster, J.M., Richardson, G. and Courtier, N.E. (2022) Ionmonger 2.0: Software for Free, Fast and Versatile Simulation of Current, Voltage and Impedance Response of Planar Perovskite Solar Cells. *Journal of Computational Electronics*, **22**, 364-382. https://doi.org/10.1007/s10825-022-01988-5

[17] Makableh, Y.F., Hassan, W., Awad, I.A. and Aljaiuossi, G. (2021) Comprehensive Electrical Modeling Analysis of Heterojunction Perovskite Solar Cells by Using Different Electron Transport Nanostructured Layers. *Superlattices and Microstructures*, **150**, Article ID: 106777. https://doi.org/10.1016/j.spmi.2020.106777

[18] Hundsdorfer, W. and Verwer, J.G. (2003) Numerical Solution of Time-Dependent Advection-Diffusion-Reaction Equations. Springer.

[19] Foster, J.M., Snaith, H.J., Leijtens, T. and Richardson, G. (2014) A Model for the Operation of Perovskite Based Hybrid Solar Cells: Formulation, Analysis, and Comparison to Experiment. *SIAM Journal on Applied Mathematics*, **74**, 1935-1966. https://doi.org/10.1137/130934258

[20] Li, D., Song, L., Chen, Y. and Huang, W. (2019) Modeling Thin Film Solar Cells: From Organic to Perovskite. *Advanced Science*, **7**, Article ID: 1901397.

https://doi.org/10.1002/advs.201901397

[21] Tessler, N. and Vaynzof, Y. (2020) Insights from Device Modeling of Perovskite Solar Cells. *ACS Energy Letters*, **5**, 1260-1270. https://doi.org/10.1021/acsenergylett.0c00172

[22] Sandberg, O.J. and Armin, A. (2019) On the Effect of Surface Recombination in Thin Film Solar Cells, Light Emitting Diodes and Photodetectors. *Synthetic Metals*, **254**, 114-121. https://doi.org/10.1016/j.synthmet.2019.06.008